Revision of *"Hail storm hazard in urban areas: identification and probability of occurrence by using a single-polarization X-band weather radar"* by *V. Capozzi, E. Picciotti, V. Mazzarella, G. Budillon, F. S. Marzano*

RC = Referee comment
AC = Authors comment
N.B. = The numbering order of the figures refers to the new version of the manuscript.

Anonymous Referee #1

RC: It is an interesting and well written paper.
AC: We thank the reviewer for her/his positive general consideration. Below you will find our answers to your comments. Moreover, we have modified the paper following his/her suggestions.

RC: Page 7 – line 2: describe in more details the error correction methodology
AC: The quality control chain applied to WR-10X data is focused on the following systematic errors: ground clutter, sea clutter, beam attenuation along the path and beam blocking by surrounding topography. The procedure is well described in Capozzi et al. (2014); anyway for your convenience you will find a summary in the following steps.

- Ground clutter rejection
  The methodologies aimed at the identification and removal of clutter echoes are based on some features with which this noise manifests itself, such as zero velocity and low spectral amplitudes (Doviak and Zrnic, 1993). Ground clutter is often associated to a field reflectivity typically much more textured than that of precipitation (Nicol et al., 2011). In the WR-10X radar a statistical declutter filter is implemented, based on the different samples distribution between clutter echoes and meteorological echoes. This filtering procedure has been improved by means of a statistical filter in order to eliminate the residual noise generated by ground clutter. The statistical filter is based on three main ingredients:
  - Entropy calculation. This step is used to recognize the radar map which deserves a filtering;
  - Texture calculations. Spatial texture basically describes the local variance of the input field. Usually high variance is associated to non-meteorological echoes
  - Median filtering. This step is applied on a Boolean mask instead of directly to the input field. This step is used to cutting out residuals spikes.

  The choice of threshold on local variance has been particularly critical: the performed analysis has suggested to adopt a lower threshold in the closer range, where the residual noise frequently occurs, and, in general, when super refraction atmospheric conditions occur.
- Sea clutter suppression
  The approach we used to suppress sea clutter noise is based on vertical reflectivity profile analysis (Alberoni et al. 2001): in rainy conditions usually vertical reflectivity profiles are smooth and regular, while in sea clutter condition a broken profile is often observed. The approach starts with vertical difference reflectivity analysis:

$$RD = Z_1 - Z_2 \quad (1)$$

where Z_1 and Z_2 are reflectivity measurements at two different antenna elevation angles above the same terrain point. A careful analysis of PPI at the lowest elevation angles showed the occurrence of sea clutter only at 1° (Capozzi et al., 2014); thus we compute RD using reflectivity data measured at 1° (Z_1) and 2° (Z_2) antenna elevation angles. Sea clutter echoes are diagnosed when one of the following conditions occur:

$$RD > T_1 \tag{2}$$

$$RD > 0 \,\&\, Z_2 < T_2 \tag{3}$$

where T_1 and T_2 are empirical threshold values.

- Path attenuation correction

Attenuation coefficient (k, dB/km) and reflectivity factor (Z, $mm^6\ m^{-3}$) are typically related by a power law:

$$k = \alpha Z^{\beta} \tag{4}$$

The two-way attenuation between two radar cells adjacent in range (A(i−1,i)) has been computed by means of Eq. 5, in which *L* is the radar bin resolution (0.3 km in our case) and Zi the non-corrected reflectivity (measured) in the i-cell.

$$A_{(i-1,i)} = 2L\,k = 2L\,\alpha Z_i^{\beta} \tag{5}$$

The literature offers many choices for α and β values: Battan (1973) suggests (α, β) = (0.00029, 0.72), Perez and Zawadzki (2003) suggest (0.000372, 0.72), while Delrieu et al. (1997) provide $0.75 \leq \beta \leq 0.85$ on the basis of an empirical approach. We mitigate attenuation issue with an iterative procedure that involves the estimation of the two-way path integrated attenuation (PIA) along the entire beam path. PIA, integrated from the radar-site to the cell i-1, can be obtained according to the formula:

$$PIA_{(0,i-1)} = \sum_{j=1}^{i-1} A_{(j-1,j)} \tag{6}$$

From Z_i, the corrected reflectivity $Z_{corr(i)}$ in i-cell can be computed according to:

$$Z_{corr(i)} = Z_i 10^{\frac{PIA(0,i-1)+A(i-1,i)}{10}} \tag{7}$$

The attenuation has been computed adopting α and β proposed by Perez and Zawadzki (2003). The algorithm just described has been tested for moderate rainfall events, in which attenuation problem can be of particular relevance. The inherent divergence of the proposed iterative algorithm is known to be an issue for convective rainfall high intensities due to the amplification of small initial errors (Delrieu et al., 1999b; Marzano et al., 2003); in this respect, a maximum threshold of PIA is set to avoid unrealistic values.

- Beam blocking by surrounding topography

The occulted percentage area of the radar beam cross section may be expressed as a function of the radius of the beam cross section, *a*, and the difference between the average altitude of the terrain and the center of the radar beam, *y* (Fig. A). According to the relative position of the beam with respect to the topography, *y* may be either negative or positive.

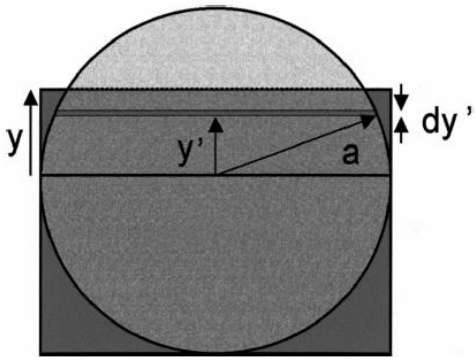

Fig. A. Elements considered in the radar beam occultation: *a*, radius of the radar beam cross section, and *y*, the difference between the center of the radar beam and the topography.

On the basis of those definitions, the partial beam blockage occurs when $-\alpha < y < \alpha$, the total beam blockage occurs when $y \geq \alpha$ and $y \leq -\alpha$ means that there is no blockage at all. Using the notation introduce above, the partial beam blockage (PBB) may be expressed as:

$$\mathrm{PBB} = \frac{y\sqrt{\alpha^2 - y^2} + a^2 \arcsin\frac{y}{\alpha} + \frac{\pi\alpha^2}{2}}{\pi\alpha} \tag{8}$$

The height of the center of radar beam, *h*, may be computed as a function of the distance *r* using the following expression (Doviak and Zrnic, 1993):

$$h = \sqrt{r^2 + (k_e R)^2 + 2\, r\, k_e\, R \sin\theta} - k_e R + H_0 \tag{9}$$

where *R* is the Earth's radius, k_e is the ratio between *R* and the equivalent Earth's radius, *E* the antenna elevation angle and H_0 the antenna height above the sea level. The term k_e contains information about the atmospheric propagation conditions and may be written as:

$$k_e = \frac{1}{1 + R\left(\frac{dN}{dh}\right)} \tag{10}$$

where *N* is the gradient of the refraction index. Substituting the (10) and (9) in (8), an expression of beam blockage in terms of propagation conditions has been obtained.

In order to minimize the effects of partial beam blockage caused by surrounding topography, we applied the correction scheme proposed by Fulton et al. (1998). This scheme is applied to beams partially obstructed, i.e. only when the level of beam occultation lies between 10% and 60%, and consists of modifying the reflectivity factor measurements by adding 1 to 4 dBZ depending on the degree of occultation.

RC: Page 9 – line 15: the content and the use of the table is not clearly understood
AC: We have modified the paper expanding the content and the use of the contingency table, also introducing the Table 4. In order to compare the outcomes of the two different radar-based hail detection techniques used in this study and the verification data (i.e. the ground truth observations), hail events have been classified using a 2-by-2 contingency table (Tab. A).

Tab. A. 2-by-2 contingency table used in the comparison between the outcomes of the two different radar-based hail detection methods and the ground truth verification data.

		Has the hail event been detected by radar?		
		YES	**NO**	
Has the hail event been observed on the ground?	**YES**	H (Hits)	M (Misses)	Total number of events observed on ground H+M
	NO	F (False Alarms)	N (Corrected Negatives)	Total number of events not observed on ground F+N
		Total number of hail events detected by radar H+F	Total number of hail events not detected by radar M+N	Total number of events H+F+M+N

The meaning of symbolisms adopted in Tab. A is explained below:

- **H (hit)** is an integer that represents the number of times that a hail event is detected by a radar-based method and is observed by ground truth reports;
- **F (false alarm)** is an integer that represents the number of times that a hail event is detected by a radar-based method and is not observed by ground truth reports;
- **M (miss)** is an integer that represents the number of times that a hail event is not detected by a radar-based method and is observed by ground truth reports;
- **N (corrected negative)** is an integer that represents the number of times that a hail event is not detected by a radar-based method and is not observed by ground truth reports.

It is assumed that a hail event is detected by a radar-based method, e.g. the WAL technique, when ΔH is above a certain threshold. In this work, in order to find the optimal warning thresholds for hail warning in Naples urban area, the contingency table has been computed for several values of ΔH, ranging from 0.2 and 3.0 km, and for several VLD values, ranging from 1.4 to 5.4 g m^{-3}.

RC: Page 9 – line 16: POD, FAR, CSI. Describe in more details the methodology for their calculation

AC: We have modified the paper following his/her suggestions: in particular, we have expanded the discussion regarding the use of the statistical scores also introducing the Table 5.

By adopting the outcomes of the 2-by-2 contingency table, the following statistical scores have been computed:

$$\text{Probability of Detection (POD)} = \frac{H}{H+M} \tag{11}$$

$$\text{False Alarm Ratio (FAR)} = \frac{F}{H+F} \tag{12}$$

$$\text{Critical Success Index (CSI)} = \frac{H}{H+M+F} \tag{13}$$

$$\text{Probability Of Hail (POH)} \equiv \frac{H}{H+F} = 1\text{-FAR} \tag{14}$$

The main features of those scores are presented in Tab. B.

Tab. B. Main peculiarities of statistical scores determined from the outcomes of the 2-by-2 contingency table.

Score	Range of values	Features	Example
POD	from 0 to 1	It is sensitive to hits (H) and does not consider the false alarms (F). It represents the fraction of hail events correctly detected by radar (H) with respect to the total number of hail events observed on ground (H+M).	POD = 0.7 means that the 70% of the hail events observed on ground has been correctly detected by radar.
FAR	from 0 to 1	It is sensitive to false alarms (F). It represents the fraction of hail events detected by radar but not observed by ground truth reports.	FAR = 0.25 means that the 25% of the hail events detected by radar has not been observed on ground
CSI	from 0 to 1	It is sensitive to both F and M. It represents the fraction of hail events observed on ground and/or detected by radar that have been correctly detected by radar.	CSI = 0.6 means that the 60% of the hail events observed and/or detected has been correctly detected by radar
POH	from 0 to 1	It is sensitive to both H and F. It represents the fraction of hail events correctly detected by radar with respect to the total number of hail events detected by radar (H+F).	POH = 0.5 means that the 50% of hail events detected by radar has been observed on ground.

RC: Page 12 – line 30: Are the WR-10X radar data available?
AC: The WR-10X radar data are available on request according to the data distribution policies of the "Campania Center for Marine and Atmospheric Monitoring and Modelling" (CCMMMA) of the University of Naples "Parthenope". For further information, please contact the Scientific Coordinator of CCMMA, Prof. Giorgio Budillon (giorgio.budillon@uniparthenope.it).

RC: technical corrections: page 7 - line 3: such as ground ... page 8 - line 3: works page 10 - line 3: concerning page 10 - line 12: cases study page 11 - line 16: rain rates up to 200 m h-1. it is better to express rainfall rate in mm/10min. page 12 - line 16: between and
AC: Many thanks for your corrections: we have implemented them in the new version of the paper.

Anonymous Referee #2

AC: We thank the reviewer for her/his comments. We have really appreciated her/his detailed reading of the manuscript. We have modified the paper following his/her suggestions. We believe that the degree of detailed analysis has reached the proper maturity. We will try to argue this conviction in the replies below.

RC: The paper describe the use of established techniques to monitor and identify hail shaft in radar echoes. The novelty could be find in the use of such techniques at X band, even if it is well recognised that attenuation play an important role at such frequency when convective storm is on the beam path. It is stated that such problem is addressed in the processing chain, a reference is present, but some doubts are not confuted since the events considered are characterised by strong convective rainfall and hail. Some additional material to demonstrate that correction is effective or a deeper discussion of its effects is not relevant is needed.
AC: The attenuation along the path, together with other sources of error, such as calibration errors, side lobe effects, shielding and range-dependent errors, can adversely affect the ability of weather radar to provide accurate measurements of vertical profile of reflectivity (Delobbe and Holleman, 2006). This issue has a significant relevance at X-band (e.g. Delrieu et al. 1999a, b) and it is strongly dependent on rain rate (Marzano et al., 2003). Nowadays, the most efficient approach to estimate the attenuation of the returning radar echoes is based on the differential phase shift between the vertical and horizontal orthogonal phases (e.g. Smyth and Illingworth, 1998), i.e. on a method that takes advantage of dual-polarization weather radar features. The weather radar tested in our work (WR-

10X), being a single-polarization system, cannot exploit polarimetric capabilities. Therefore, in the framework of the quality control chain applied to correct WR-10X reflectivity measurements, the beam attenuation along the path has been mitigated through a classical iterative procedure that involves the estimation of two-way path integrated attenuation (PIA) along the entire beam path. This iterative algorithm, whose detailed description is provided in this document at page 2, has been tested for strong and moderate rainfall events, in which path attenuation problem can be of particular relevance (Capozzi et al., 2014). The PIA method proved to be fairly reliable in attenuation correction within a range (i.e. distance from the radar site) less than 50 km; occasional failures of this methodology have been observed in the case of particular meteorological scenarios, characterized by moderate and persistent rainfall in the range closest to the radar site due to the fast accumulation of path two-way path beam extinction.
Indeed, in the specific context of our study the influence of attenuation on radar-based hail detection techniques performance may be considered relatively low for two main reasons:
1. The radar-based hail detection products developed in this work have been tested at urban scales of the order of few tens of kilometers. The occurrence of path attenuation along specific radial directions may be considered relatively rare at short ranges (Marzano et al., 2012) and, therefore, not affecting the performance of X-band radars, at least in a statistical sense;
2. In the selection of thunderstorm events, in order to minimize the effects of attenuation, we have focused on situations where no other convective cells are present along the radial directions between the radar site and the convective cell of interest. In this respect, a nice example is given just by the case study analyzed in the Section 4.3: no other precipitation patterns are present, along the radial directions, between the radar site and the convective cell which affected the Sorrentine Peninsula.
The attenuation issue could be mitigated also in critical situation (i.e. when this phenomenon is experienced along radial observations in convective rainfall), exploiting a composite X-band radar network configuration, which is able to detect the precipitation patterns from two (or more) points of view.
All these arguments have been reported in the revised version of the paper.

RC: 1) 2.1 Waldvogel method. In this section the Waldvogel method is presented. In such method an important role is played by the Ht0 variable. I suggest to move here (e.g. at the end of the section) the discussion on how such variable is computed. Does not make sense to have this discussion in the presentation of the radar (sect. 3.1). It could be beneficial to add a discussion on the estimate of the error in the interpolation and the sensitivity of the algorithm to such error.
AC: Following the suggestion of the referee, we have moved the discussion of the calculation of the height of freezing level (H_{T0}) at the end of section 2.1. Moreover, we have added a discussion about the estimate of the error in linear interpolation of vertical temperature profiles measured by atmospheric soundings.
The error (E) in linear interpolation of a determined function $f(x)$ can be generally defined as:

$$E = f(x) - p(x) \tag{15}$$

Where p denotes the linear interpolation polynomial between the interval (x_0, x_1). $p(x)$ is defined as follow:

$$p(x) = f(x_0) + \frac{f(x_1)-f(x_0)}{x_1-x_0}(x - x_0) \tag{16}$$

It can be demonstrated, using the Rolle's theorem, that if f has a continuous second derivative, E is bounded by:

$$|E| \leq \frac{(x_1-x_0)^2}{8} \max_{x_0 \leq x \leq x_1} |f''(x)| \tag{17}$$

According to Eq. (17), the linear interpolation between two points of a given function gets worse with the second derivative of the function that is approximated.
Therefore, we have used Eq. (17) to estimate the maximum error for linear interpolation of vertical temperature profiles measured by atmospheric soundings. In our case, $f(x)$ denotes the air-temperature, expressed in °C, which is dependent from the height x, also measured by radiosondes

and expressed in meters. Errors referring to the freezing point altitude range are discussed. In particular, we show results obtained for the interval (x_0, x_1), with x_0 and x_1 being respectively the altitudes where air-temperature is immediately above and below the freezing level. The frequency distribution of the error bound for the linear interpolation of air-temperature data in this interval is presented in Fig. B.

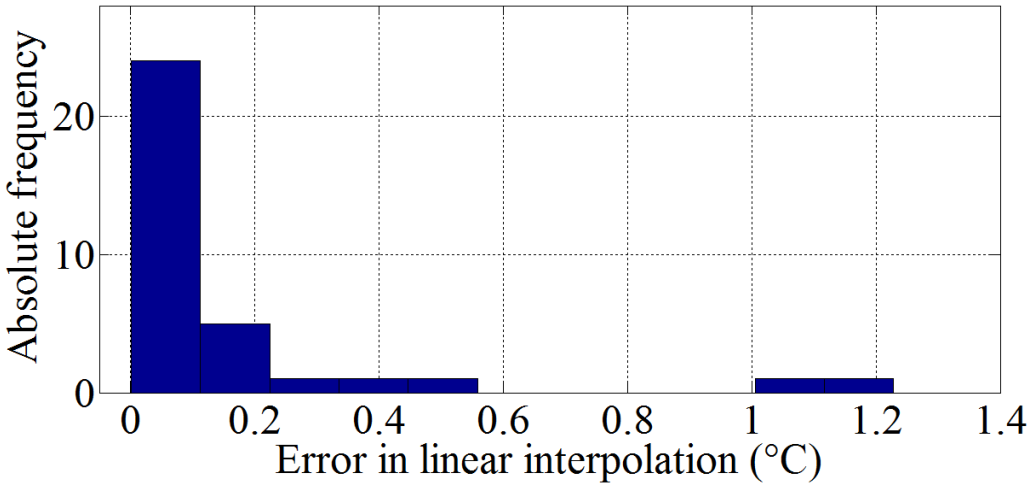

Fig. B: Frequency distribution of error bound for linear interpolation of temperature data measured by atmospheric soundings in the altitudes interval (x_0, x_1) where the freezing level is located.

The magnitude of error bound is generally lower than the total uncertainty in sounding (0.5°C) of the radiosonde Vaisala RS92-SG temperature sensor used in Pratica di Mare station (Hurst et al., 2011). Therefore, the impact of error bound on the performance of WAL method can be considered negligible. However, the frequency distribution reveals rare cases in which the error in linear interpolation of atmospheric sounding's temperature data exceeds the value of 1.0°C. As worst scenario, we considered the event in which the highest error bound (1.1°C) has been found. Assuming a temperature decrease with height at the average lapse rate of 6.5°C per kilometer, an error in air-temperature estimation of ± 1.1°C would result in an error of the altitude assigned to the freezing level of about ± 169 m. This error can determine a variation of POH_{WAL} index of about ± 1%. Therefore, also in the worst scenario, the sensitivity of WAL algorithm to the error in linear interpolation of atmospheric sounding data may be considered negligible.

RC: 2) pag. 8 – row 8-15. Could be useful to report on a map where the events are located (hail reports).
AC: We are grateful to the referee for this suggestion. We have produced a map that includes the location of the 34 hail events. This map, added in the new version of the paper, contains also information about the verification data type (volunteers report, synop observation and local newspapers).

RC: 3) pag 8 from row 25 to the end of section 3.2 The text in this section of paragraph 3.2 reports some convection initiation mechanisms, but since no previous work are referred neither there is an analysis that support such mechanisms I have to assume that this is an authors's inference. Since this is not relevant for the paper I suggest to remove it. Alternatively add a section to demostrate such processes.
AC: According to the suggestions of the referee, we have decided to remove the section of paragraph 3.2 that reports some convection initiation mechanism typical of the western sector of Campania Region.

RC: 4) pag 10 - row 14 Could you clarify what you have used as dependent variable and independent variable in the fitting curve? I assume that you use POH and H for Wal and POH

and VLD for VLD. If this is correct could you explain why you need another way to calculate POH ? Is is related to error in POH estimate? Please clarify.
AC: The two POH indexes (POH_{WAL} and POH_{VLD}) should not be intended as an alternative way to compute the POH score, but as operational radar-based hail detection products derived through a heuristic approach, similar to the POH index derived in Holleman (2001). In order to determine a POH index that can be easily used into an operative framework to assess the hail warning in Naples urban area, we modeled the relationship between POH score and the radar products (ΔH for WAL method and VLD for VIL-Density method) by using a third-order polynomial fit. We set up the polynomial model using POH score as dependent variable and the radar product (ΔH or VLD) as independent variable, highlighting this point in the revised paper.

RC: 5) Pag 10 – rows 21-22 Could you please explain how such threshold have been calculated?
AC: The two optimal values for hail warning in Naples urban area, $POH_{WAL} = 0.87$ and $POH_{VLD} = 0.76$, correspond, respectively, to ΔH ($= H_{Z40} - H_{T0}$) and VLD warning thresholds identified in the framework of statistical analysis, discussed in the paragraph 4.2. More specifically, we used the maximum value of Critical Success Index (CSI) as criterion to assess the hail warning thresholds. For WAL method, the maximum CSI value corresponds to $\Delta H = 1.0$ km; in the same manner, for VIL-Density method, the maximum CSI value corresponds to VLD = 2.4 g m^{-3}. We have better clarified that in the revised version of the paper.

RC: 6) Pag 11 row 5 Substitute "bottom panel" with "right panel"
AC: Following the referee suggestion, we have replaced "bottom panel" with "right panel". We really apologize for the typo.

RC: 7) pag 11 row 12 Add a marker for Vico Equense on the map
AC: Following the referee recommendation, we have added a marker for Vico Equense city in Fig. 10.

RC: 8) pag 11 row 16 Add a reference to the local newspaper
AC: Following the referee suggestion, we have added the reference to the local newspaper (Il Mattino, July 21, 2014). We really apologize for this omission.

RC: 9) page 11 row 32 There is no clear indication that hail information is "precise about time and location". Remodulate the sentence
AC: We have remodulated the sentence in the following manner: "The dataset used in this work includes 53 thunderstorm events, occurred in the study area between April 2012 and June 2015. The information about hail phenomena at ground level have been collected using the observations provided by three synop stations, the volunteer's reports and the newspapers. Due to the small spatial and temporal extent of most hail events, the latter two sources of information proved to be very useful to generate a sufficiently large dataset of on-ground hail observations".

RC: 10) Table 3 Is the mean the significative parameter for the distribution of the quantities used? Add information about distributions (at least in the replay)
AC: The average value of the parameters listed in Table 3 may be useful to highlight some seasonal-dependent features of thunderstorm events that occurred in the study area. As discussed in the paragraph 3.2, warm season (May to October) events, developing in a moist and warm environment, exhibit a deeper vertical extension than cold season (November to April) events and, consequently, are more prone to produce dangerous hailstones.
However, the doubts about the significance of the average value are licit, especially considering that the seasonal analysis "reduce" the sample size. Therefore, following the referee's suggestions, we computed the frequency distribution for every parameter presented in Table 3. Fig. C and Fig. D show the results obtained for warm and cold season, respectively. In order to evaluate the results from a

quantitative perspective, we determined also the main statistical properties (average, standard deviation, skewness and kurtosis) of the radar-based products: the results are presented in Tab. C (warm season) and Tab. D (cold season).

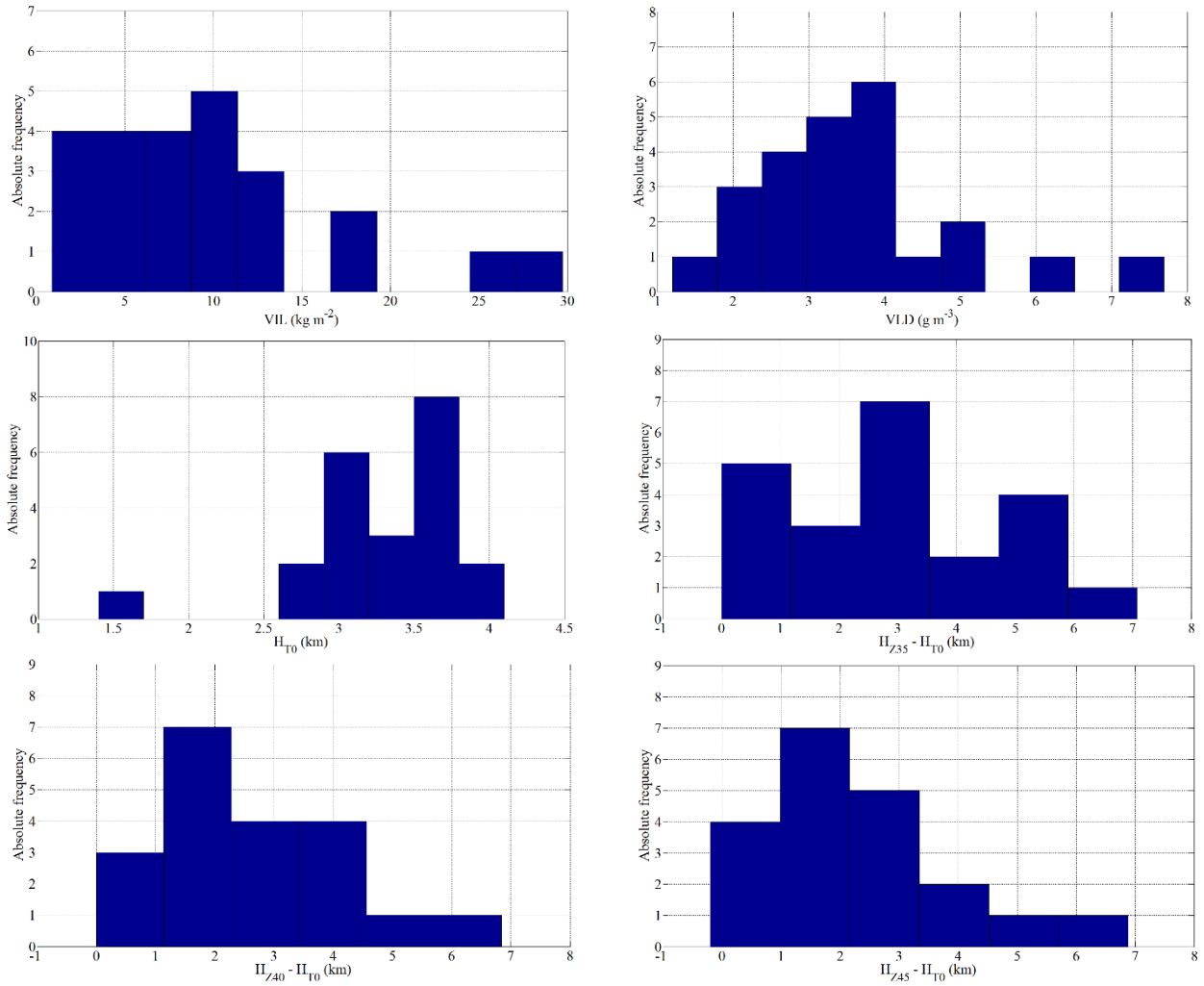

Fig. C. Frequency distribution of some products generated by the two radar-based hail detection methods. Only warm season events are considered.

Tab. C. Main statistical properties (Average, Standard Deviation, Skewness and Kurtosis) of some products generated by the two radar-based hail detection techniques. Only warm season events are considered.

Parameter	Average	Standard deviation	Skewness	Kurtosis
VIL (kg m^{-2})	9.5	6.8	1.1	3.8
VLD (g m^{-3})	3.6	1.4	0.8	3.7
H_{T0} (km)	3.2	0.5	-1.9	7.5
$H_{Z35} - H_{T0}$ (km)	2.7	1.8	-0.02	1.9
$H_{Z40} - H_{T0}$ (km)	2.5	1.6	0.1	2.2
$H_{Z45} - H_{T0}$ (km)	2.2	1.6	0.5	2.6

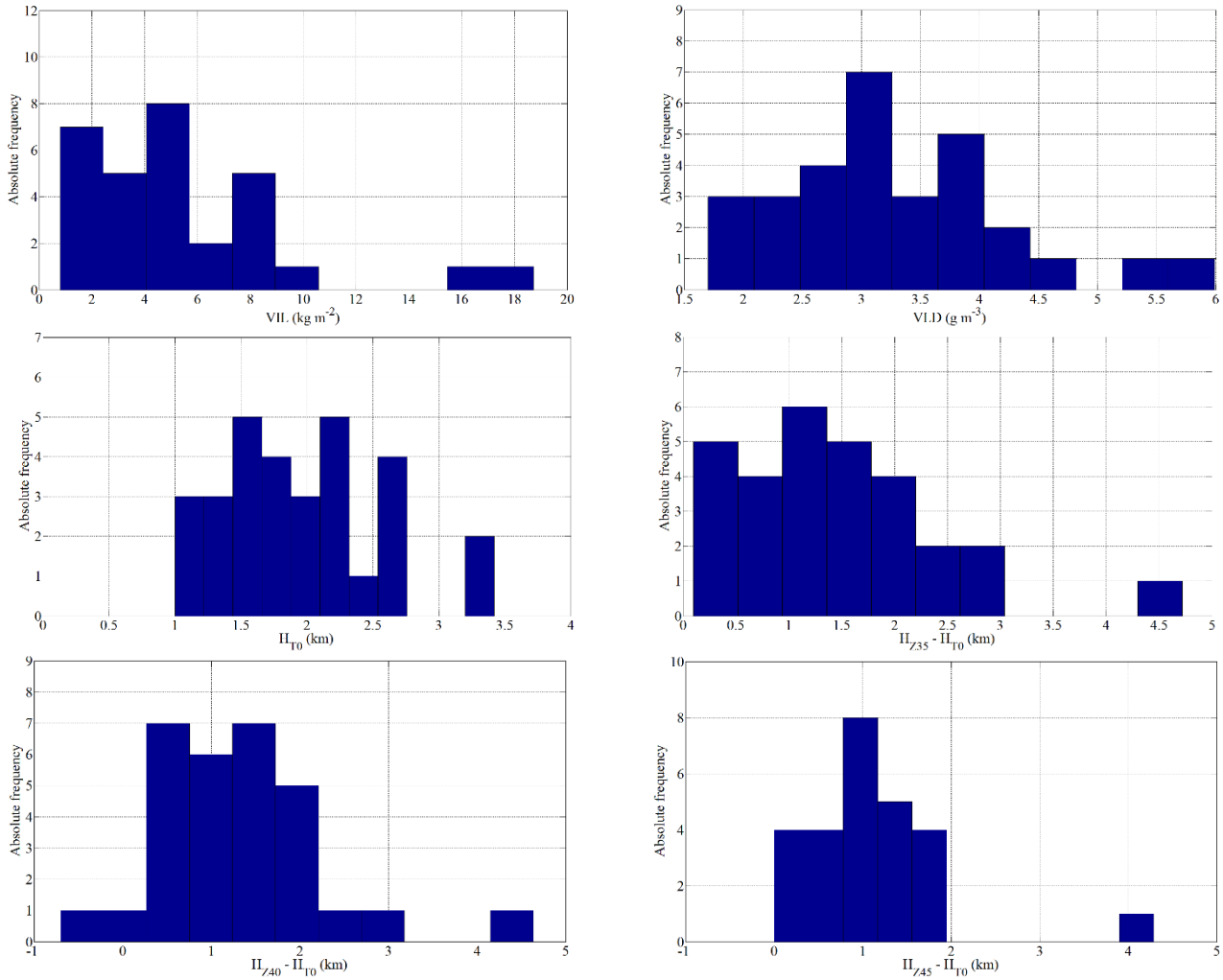

Fig. D. Frequency distribution of some products generated by the two radar-based hail detection methods. Only cold season events are considered.

Tab. D. Main statistical properties (Average, Standard Deviation, Skewness and Kurtosis) of some products generated by the two radar-based hail detection techniques. Only colds season events are considered.

Parameter	Average	Standard deviation	Skewness	Kurtosis
VIL (kg m^{-2})	5.2	3.9	1.5	5.3
VLD (g m^{-3})	3.1	0.9	0.6	3.1
H_{T0} (km)	1.9	0.6	0.4	2.3
$H_{Z35} - H_{T0}$ (km)	1.4	0.9	0.9	4.4
$H_{Z40} - H_{T0}$ (km)	1.3	0.9	0.7	4.6
$H_{Z45} - H_{T0}$ (km)	1.1	0.7	1.8	8.2

As concerning warm season, VIL, VLD and H_{T0} frequency distributions exhibit a great asymmetry (positive for VIL and VLD, negative for H_{T0}); in addition, kurtosis value suggests that those distributions are leptokurtic, i.e. they are characterized by a high and sharp peak and, at the same time, by long tails. The outputs of WAL method show a frequency distribution approximatively symmetric (except for $H_{Z45} - H_{T0}$, in which case a moderate positive asymmetry has been detected) and platykurtic, i.e. the central peak is broader and lower and the tails are shorter. In cold season, all quantities exhibit a moderate or high positive asymmetry and a large kurtosis (except for H_{T0}). Therefore, the results of this analysis highlight that the radar-based hail detection products listed in Table 3 are moderate or extremely non-normally distributed. In order to have a better measure of

central tendency, we propose the use of the median, which is typically preferred to average for skewed data distribution

RC: 11) fig 7 Both panels are not clear, try to improve they
AC: Following the reviewer suggestion, we have tried to improve the panels of Fig. 9 by enlarging their size.

RC: 12) Fig. 8 and fig 10 increase the level of zoom used. It is hard a good analysis from this picture. It is not easy identify where hail expected and where not. This open a question on the identification of the hailfall location. Is the area, above threshold, much bigger that the area from the reports? If yes could you comment it?
AC: Following the referee suggestion, we have enlarged the size of Fig. 10 and Fig. 12. Moreover, we have provided a better display of the areas where hail is expected according to the two POH indexes (POH_{WAL} and POH_{VLD}) through the maps presented in Fig. E. The areas where hail is likely to occur (i.e. where the POH index is above the warning threshold) are highlighted in red.

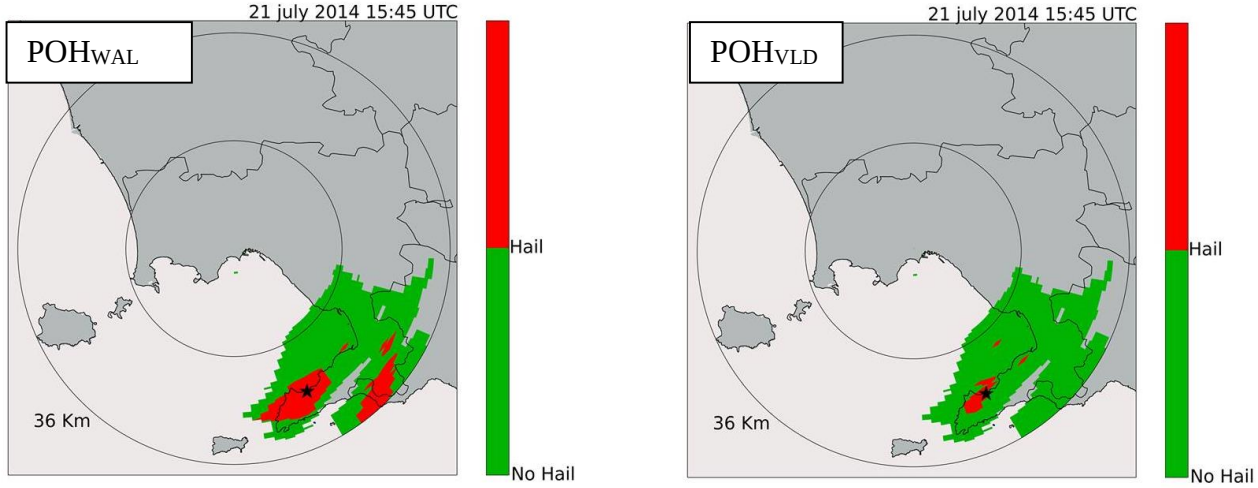

Fig. E: Probability of Hail obtained by WR-10X when the hailstorm passed over Sorrento city (highlighted by black star). The areas where hail is likely to occur (i.e. where the POH index is above the warning threshold) are indicated in red, the areas where hail is not expected (i.e. where the POH index is below the warning threshold) in green. In the left panel, the results obtained from WAL method are presented; in the right panel, those obtained from VIL-Density method are displayed.

The two radar-based hail detection products, developed in this study, identify an area where hail is expected which includes the city of Sorrento and the adjacent zones. In this case, such result should not be interpreted as a partial fault of the two algorithms, but, indeed, as a further evidence of their reliability. In fact, the hailstorm occurred on July 21, 2014 affected a large part of the Sorrentine Peninsula. Although the ground truth reports provided by local newspaper (comprehensive of photographic and video material) were all collected in Sorrento city, there is a reliable evidence that hail precipitation affected also the municipalities neighbouring Sorrento (Massa Lubrense, Sant'Agnello, Meta di Sorrento, Piano di Sorrento and Vico Equense). As reported by local newspapers (Positano News, July 28, 2014), those municipalities declared a state of natural disaster due to the huge damages and losses caused by hailfall on July 21, 2014.
On a more general level, the issue addressed by referee is one of the major limitation in the framework of the evaluation of radar-based hail identification products performance as a systematic ground validation of hailfall is always a difficult task. The uncertainty about the occurrence over a larger area still remains and cannot be resolved with the information and data at disposal.
In the case study shown the two radar-based hail detection methods identify two different areas (in terms of size) where hail is most likely expected. Even though using different algorithms to determine

the two POH indexes, both radar-based products correctly detect the hail occurrence in the area where hail has been actually reported on ground.

Cited references

- Alberoni, P. P., Andersson, T., Mezzasalma, P., Michelson, D. B., and Nanni, S.: Use of the vertical Reflectivity profile for Identification of Anomalous propagation, Meteorol. Appl., Vol. 8 (3), pp. 257 – 266, 2001.
- Battan, L. J.: Radar Observation of the Atmosphere, University of Chicago Press, pp. 324, 1973.
- Capozzi, V., Picciotti, E., Budillon, G., and Marzano, F.S.: X-band weather radar monitoring of precipitation fields in Naples urban areas: data quality, comparison and analysis, The Eighth European Conference On Radar in Meteorology and Hydrology, 2014.
- Delobbe, L. and Holleman, L.: Uncertainties in radar echo top heights used for hail detection, Meteorol. Appl., Vol. 13, pp. 361-374, 2006.
- Delrieu, G., Caoudal, S., and Creutin, J.D.: Feasibility of using mountain return for the correction of ground-based X-band weather radar data, J. Atmos. Oceanic Technol., Vol. 14, pp. 367–385, 1997.
- Delrieu, G., Hucke, L., and Creutin, J.D.: Attenuation in Rain for X- and C-Band Weather Radar Systems: Sensitivity with respect to the Drop Size Distribution, Journal of Applied Meteorology, Vol. 38, pp. 57-68, 1999a.
- Delrieu, G., Serrar, S., Guardo, E., and Creutin, J.D.: Rain Measurement in Hilly Terrain with X-Band Weather Radar Systems: Accuracy of Path-Integrated Attenuation Estimates Derived from Mountain Returns, J. Atmos. Oceanic Technol., Vol. 16, pp. 405–416, 1999b.
- Doviak, R., and Zrnic, D.: Doppler radar and weather observations, Academic Press UK, pp. 592, 1993.
- Fulton, R.A., Breidenbach, J.P., Seo, D., Miller, D., and O'Bannon, T.: The WSR- 88D Rainfall Algorithm, Wea. Forecasting, Vol. 13, pp. 377-395, 1998.
- Holleman, I.: Hail detection using single-polaritazion radar, Scientific Report, KNMI WR-2001-01, 2001.
- Hurst, D. F., Hall, E. G., Jordan, A. F., Miloshevich, L. M., Whiteman, D. N., Leblanc, T., Walsh, D., Vömel, H., and Oltmans, S. J.: Comparisons of temperature, pressure and humidity measurements by balloon-borne radiosondes and frost point hygrometers during MOHAVE-2009, Atmos. Meas. Tech., 4, 2777-2793, doi:10.5194/amt-4-2777-2011, 2011.
- Il Mattino: Grandinata record a Sorrento, i chicchi enormi danneggiano i campi, retrieved from, http://www.ilmattino.it/napoli/cronaca/grandinata_sorrento_foto_video-508584.html, July 21, 2014.
- Marzano, F.S., Roberti, L., Di Michele, S., Tassa, A., and Mugnai, A.: Modeling of apparent radar reflectivity due to convective clouds at attenuating wavelengths, Radio Sci., Vol. 38, No. 1, pp. 1002, 2003.
- Marzano, F.S., Budillon, G., Picciotti, E., Montopoli, M., Zinzi, A., and Buonocore, B.: X-band weather radar monitoring real-time products in Rome and Naples urban areas. Tyrrhenian Workshop 2012 on Advances in Radar and Remote Sensing, 2012.
- Nicol, J.C., Illingworth, A.J., Darlington, T., and Sugier, J.: Techniques for improving ground clutter identification, Weather radar hydrology: proceedings of a symposium held in Exeter, UK, April 2011, IAHS Publ. 3XX, 2011.
- Perez, M.A., and Zawadzki, I.: S- and X-band dual-wavelength radars revisited, Preprints, 31st Int. Conf. on Radar Meteorology, Seattle, WA, Amer. Meteor. Soc., pp. 51–54, 2003.
- Positano News: Sorrento grandinata del 21 luglio i comuni chiedono lo stato di calamità, retrieved from http://www.positanonews.it/articolo/141289/sorrento-grandinata-del-21-luglio-i-comuni-chiedono-lo-stato-di-calamita, July 28, 2014.
- Smyth, T.J. and Illingworth, A.J.: Correction for attenuation of radar reflectivity using polarization data, Quarterly Journal of the Royal Meteorological Society, Vol. 124, Issue 551, pp. 2393–2415, Oct. 1998 Part A.